Satellite Navigation
https://satellite-navigation.springeropen.com/

ORIGINAL ARTICLE

Open Access

Underwater inertial error rectification with limited acoustic observations

Hongqiong Tang[1], Hongyang He[1], Fangneng Li[1*] and Jiangning Xu[1]

Abstract

Underwater inertial navigation is particularly difficult for the long-durance operations as many navigation systems such global satellite navigation systems are unavailable. The acoustic signal is a marvelous choice for underwater inertial error rectification due to its underwater penetration capability. However, the traditional Acoustic Positioning Systems (APS) are expensive and incapable of positioning with limited acoustic observations. Two novel underwater inertial error rectification algorithms with limited acoustic observations are proposed. The first one is the single acoustic-beacon Range-only Matching Aided Navigation (RMAN) method, which is inspired by matching navigation without reference maps and presented for the first time. The second is the improved single acoustic-beacon Virtual Long Baseline (VLBL) method, which considers the impact of indicated relative position increments on virtual beacon reconstruction. Both RMAN and improved VLBL are further developed when multi acoustic-beacons are available, named mAB-RMAN and mAB-VLBL. The comprehensive simulations and field investigations were conducted. The results demonstrated that the proposed methods achieved excellent accuracy and stability compared to the baseline, specifically, the mAB-RMAN and mAB-VLBL can reduce the inertial error by more than 90% and 98% when using single and double acoustic-beacons, respectively. These proposed techniques will provide new perspectives for underwater positioning, navigation, and timing.

Keywords Underwater PNT, Range-only matching aided navigation, Virtual long baseline, Inertial error rectification

Introduction

The increasing marine exploration and activities have placed high demands on underwater Positioning, Navigation and Time (PNT). Unlike aerial and land navigation, the Global Satellite Navigation Systems (GNSS) is unavailable underwater due to its poor penetration capability (Yang, 2018). Typical underwater positioning and navigation techniques include Inertial/Dead Reckoning Navigation System (INS/DRNS) (El-Sheimy & Youssef, 2020; Paull et al., 2014), Acoustic Positioning Systems (APS) (Qin et al., 2022; Tang et al., 2023; Zou et al., 2023), and Geophysical Matching Aided Navigation (GMAN) using gravity, terrain, and magnetic (Wang et al., 2023; Zhang et al., 2022), and etc.. However, an individual positioning and navigation method is often insufficient to meet the demands of underwater PNT for the activities such as ocean exploration, monitoring, and military operations (Yang & Qin, 2021), particularly for the long-duration and long-distance underwater missions (Xu, 2017).

Underwater positioning commonly utilizes inertial-acoustic integrated navigation, which combines Inertial Navigation System (INS) and APS (Claus et al., 2018; Liu et al., 2021; Masmitja et al., 2019; Wang et al., 2022a, 2022b; Zou et al., 2023). Inertial navigation provides self-sufficiency, concealment, and all-around output with a high rate, but it is prone to accumulating errors over time, which needs external position correction periodically. The Doppler Velocity Log (DVL) has limitations in deep-sea areas and can only measure the velocity relative to water (Wang et al., 2020). INS/DVL integrated

*Correspondence:
Fangneng Li
fnli_nue@163.com
[1] Department of Navigation Engineering, Naval University of Engineering, Wuhan 430000, China

navigation only partially restrains INS errors and cannot guarantee bounded positioning errors (Tang et al., 2023). Acoustic positioning includes Long Baseline (LBL), Short Baseline (SBL), Ultra-Short Baseline (USBL), and single acoustic-beacon range-only positioning. LBL measures the Round-Trip Time (RTT) to perform triangulation on vehicle using asynchronous query-response. A typical LBL system includes multi acoustic-beacons that need calibration and supervision (LaPointe, 2006). It is an expensive and time-consuming task, particularly during large-scale underwater operations in multiple areas that require separate deployment, calibration, and recovery for the acoustic-beacons (Masmitja et al., 2019). Additionally, LBL's query-response approach restricts the acoustic-beacons service capacity and cannot work for multiple underwater vehicles in parallel. Moreover, complicated underwater environments may limit acoustic observations that needs improving to meet the requirement for the triangulation.

Due to its simple structure and considerable scalability, the single acoustic-beacon range-only navigation has attained increasing attention (Jakuba et al., 2021; Rypkema et al., 2018; Zhao et al., 2022). The One-Way Travel Time (OWTT)-based passive inverted USBL (piUSBL) system estimates the OWTT slant range and azimuth by acquiring broadcast signals from a time-synchronized acoustic-beacon (Wang, et al., 2022a). However, the piUSBL system has limited potential to support high-accuracy positioning in extensive operating spaces as the restricted size of the receiver. The filter-based range-only navigation techniques correct the position errors of the vehicle by employing extended Kalman filters or particle filters as estimators while taking the slant range as observation (Jankovic et al., 2023; Masmitja et al., 2019). Most filter-based methods rely on linearized error models, prior system knowledge, and measurement noise (Claus et al., 2018). Unreasonable linearized error models or filter parameter settings may cause the filter diverge. The Virtual/Synthetic Long Baseline navigation (VLBL/SLBL) technique is commonly used in single acoustic-beacon range-only navigation (LaPointe, 2006; Scherbatyuk, 1995). The SLBL approach can be developed for mobile LBL systems (Vaganay et al., 2004; Webster et al., 2012) for cooperative navigation with the help of reliable acoustic communication (Huang et al., 2018). In these systems, the acoustic beacons are fixed on the leader equipped with a high-precision navigation system, and their positions are broadcast to other vehicles through acoustic communication. This method offers excellent flexibility, but it does result in a higher system cost and may impact the system concealment.

The existing literature has primarily assumed that the indicated Relative Position Increment (RPI) is reliable for constructing virtual beacons and achieving VLBL positioning. However, this assumption is not always accurate, especially when the vehicle enters the functional area of the acoustic-beacon after a long-duration snorkeling. Both heading and scale errors will directly affect the position accuracy of virtual beacons. Traditional VLBL algorithms cannot eliminate these errors, and increasing the length of observations will also not improve algorithm accuracy. To our best knowledge, no publicly available literature reported the VLBL, which considers the indicated-RPI error.

The GMAN utilizes the intrinsic (slowly varying) physical features of the Earth for navigation purposes (Wang et al., 2023; Zhang et al., 2022). This kind of navigation exhibits the features such as all-weather capability, strong concealment, and non-accumulative error. The GMAN maximizes the correlation between the retrieved and measured sequences by matching the indicated track with the most suitable track in a pre-collected background reference map. Traditional matching aided algorithms include Terrain Contour Matching (TERCOM), Iterative Closest Contour Point (ICCP), and Sandia Inertial Terrain-Aided Navigation (SITAN). Among them, the ICCP-based algorithm maintains the advantages of TERCOM and SITAN algorithms. It addresses their shortcomings, such as the linearization of terrain required by SITAN and the accurate yaw information required by TERCOM. However, establishing high-resolution background maps for the GMAN requires expensive and labor-intensive effort and the deployment of costly measurement instruments like gravity meters on underwater vehicles. Furthermore, its matching aided navigation accuracy is limited, restricting its extensive application.

Motivated by the limitations mentioned above, this work aims at inertial error rectification with limited acoustic observations. For clarity, an abbreviation list with full explanations is given in abbreviation. The main contributions of this paper are as follows:

1. A single Acoustic-Beacon (sAB-) Range-only Matching Aided Navigation (RMAN) algorithm, inspired by the GMAN without a reference map, is presented. It is the first-ever incorporation of matching aided navigation into range-only navigation, potentially opening up new perspectives in underwater navigation.
2. An improved sAB- VLBL algorithm considering the system-indicated RPI error (both rotational and scaling) is investigated.
3. Both sAB-RMAN and improved sAB-VLBL are further developed to accommodate the wider conditions with multi acoustic-beacons, denoted as

mAB-RMAN and mAB-VLBL, and achieve higher reliability.
4. Comprehensive simulation and field tests are conducted to evaluate the proposed algorithms and the results show excellent accuracy and stability are obtained compared to the baselines.

The remainder of this paper is organized as follows. Preliminaries are presented first. Section "Acoustic-beacon range-only matching aided navigation" derived the sAB-RMAN and mAB-RMAN. The details of sAB-VLBL and mAB-VLBL are provided in the "Improved VLBL by considering indicated-RPI error" section. Comprehensive simulation and field tests are conducted in the "Performance verification" section. Conclusion and future work are given in the last section.

Preliminaries

We use upper (lower) bold-face letters to denote matrices (vectors). An $n \times n$ identity matrix will be marked as $\boldsymbol{I}_n$. The special group $\mathcal{SO}(n) := \{\boldsymbol{A} \in \mathbb{R}^{n\times n} | \boldsymbol{A}\boldsymbol{A}^{\mathrm{T}} = \boldsymbol{I}_n, \det\boldsymbol{A} = 1\}$ is rotation matrices in $\mathbb{R}^n$, where det is for the determinant. $\boldsymbol{A}_i$ is the i-th row of matrix $\boldsymbol{A}$. The operators $|\cdot|$ and $||\cdot||$ are the L_1 and L_2 norms. Given $\vartheta \in [0, 2\pi)$, we define the unit orthonormal vectors $\boldsymbol{w}_\vartheta := [\cos(\vartheta) \ \ \sin(\vartheta)]^{\mathrm{T}}$,$\boldsymbol{w}_\vartheta^\perp := [-\sin(\vartheta) \ \ \cos(\vartheta)]^{\mathrm{T}}$, and define the map $f : \vartheta \mapsto \boldsymbol{R}_\vartheta := [\boldsymbol{w}_\vartheta \ \ \boldsymbol{w}_\vartheta^\perp] \in \mathcal{SO}(2)$. The *body*, *navigation*, *earth,* and *inertial* frame are denoted by lower letters *b*, *n*, *e,* and *i*, respectively. The "East (E)-North (N)-Up (U)" frame plays as the *n*-frame in this paper. Denote $\boldsymbol{R}_b^n \in \mathcal{SO}(3)$ as the *attitude* matrix from *b*-frame to *n*-frame, the $\boldsymbol{v}_{eb}^n = [v_{eb,\mathrm{E}}^n \ \ v_{eb,\mathrm{N}}^n \ \ v_{eb,\mathrm{U}}^n]^{\mathrm{T}}$ as *velocity*, and the $\boldsymbol{p}^n = [L \ \ \lambda \ \ h]^{\mathrm{T}}$ as *position* in *n*-frame, where L, λ and h is the *latitude*, *longitude,* and *height,* respectively.

Inertial/dead reckoning navigation system

The Strapdown Inertial Navigation System (SINS) kinematics can be described in terms of attitude, velocity, and position (Chang et al., 2023).

$$\begin{cases} \dot{\boldsymbol{R}}_b^n = \boldsymbol{R}_b^n(\boldsymbol{\omega}_{ib}^b\times) - (\boldsymbol{\omega}_{in}^n\times)\boldsymbol{R}_b^n \\ \dot{\boldsymbol{v}}_{eb}^n = \boldsymbol{R}_b^n\boldsymbol{f}_{ib}^b - (2\boldsymbol{\omega}_{ie}^n + \boldsymbol{\omega}_{en}^n)\times\boldsymbol{v}_{eb}^n + \boldsymbol{g}_{ib}^n \\ \dot{\boldsymbol{p}}^n = \boldsymbol{R}_c\boldsymbol{v}_{eb}^n \end{cases} \tag{1}$$

where $\boldsymbol{\omega}_{ib}^b$ is the body angular rate expressed in the *b*-frame w.r.t the *i*-frame, measured by gyroscopes with inevitable drift, bias, and random noise. $\boldsymbol{\omega}_{in}^n$ is *n*-frame angular rate w.r.t *i*-frame, $\boldsymbol{\omega}_{ie}^n = [0 \ \ \omega_{ie}\cos L \ \ \omega_{ie}\sin L]^{\mathrm{T}}$ is the earth angular rate expressed in *n*-frame w.r.t the *i*-frame and ω_{ie} is the earth rotation rate. $\boldsymbol{\omega}_{en}^n$ is *n*-frame angular rate expressed in *n*-frame w.r.t *e*-frame. $\boldsymbol{f}_{ib}^b$ is the specific force measured by accelerometers. $\boldsymbol{g}_{ib}^n$ is the gravity vector in *n*-frame. The matrix $\boldsymbol{R}_c$ is the local curvature matrix.

The $\boldsymbol{p}^n$ is not strictly belongs to Euclidean space and can be converted to the Cartesian coordinate system by

$$\boldsymbol{p}^e = \ell(\boldsymbol{p}^n) = \begin{pmatrix} (R_N + h)\cos L\cos\lambda \\ (R_N + h)\cos L\sin\lambda \\ R_N[(1 - e_1^2) + h]\sin L \end{pmatrix} \tag{2}$$

where R_N is the transverse radius of curvature of the WGS-84 reference ellipsoid.

The underwater vehicle position can also be obtained by a Dead Reckoning Navigation System (DRNS)

$$\dot{\boldsymbol{p}}^n = \kappa\boldsymbol{R}_c\boldsymbol{R}_b^n\boldsymbol{R}_d^b\boldsymbol{v}_{bd}^d \tag{3}$$

where $\boldsymbol{v}_{bd}^d$ is the ground velocity measured by DVL and expressed in DVL frame (*d*-frame) w.r.t *b*-frame. $\boldsymbol{R}_d^b \in \mathcal{SO}(3)$ is the constant misalignment attitude transformation matrix from *d*-frame to *b*-frame. κ is the scale factor of DVL. They can be calibrated in advance (Li et al., 2022). $\boldsymbol{R}_b^n$ is the attitude transformation matrix and can be determined by a gyrocompass or Inertial Measurement Unit (IMU).

In the following derivations, an underwater Two Dimensional (2D) scenario will be employed as the Three Dimensional (3D) slant-range measured by acoustic modems can be transformed into a 2D range by incorporating the vehicle's depth provided with pressure sensor and the prior knowledge of the depth of the acoustic-beacon.

Virtual long baseline

The VLBL navigation algorithm enables an underwater vehicle to determine its globally referenced position using an external single acoustic-beacon with a known global position (LaPointe, 2006). As shown in Fig. 1 with colored version, by manipulating multiple asynchronous ranges from the same acoustic-beacon, a long baseline of virtual beacons situated in various locations at a single point in time is created. Consequently, the underwater vehicle computes its global location using these virtual beacons like the method employed in a traditional LBL system.

Based on the geometric relationship between the virtual beacons and the vehicle, the acoustic observation equations can be derived as

$$r_i = \left\|\boldsymbol{x}_N - \boldsymbol{p}_{v,i}\right\| = \sqrt{R_i^2 - \Delta h_i^2} \ , \quad i = 1, ..., N. \tag{4}$$

where $R_i = c\Delta t_i \in \mathbb{R}$ is the ith 3D slant-range between the physical beacon and the vehicle position, r_i is the 2D range, c is the Effective Sound Velocity (ESV), Δt_i is the OWTT, Δh_i is the depth difference between the vehicle and the single acoustic-beacon, and $\boldsymbol{x}_N$ is the current

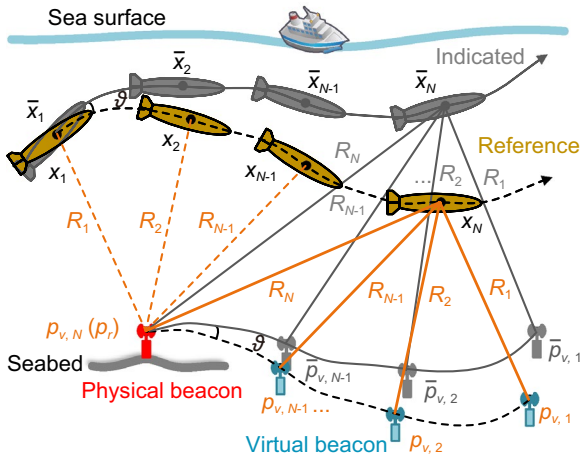

Fig. 1 The principle of VLBL (The colored version represents the indicated-RPI is error-free while grey one better reflects the practical scenario)

position to be solved. The location of the i-th virtual beacon $\mathbf{p}_{v,i}$ can be denoted as

$$\boldsymbol{p}_{v,i} = \boldsymbol{p}_r + \Delta \boldsymbol{x}_i^N \tag{5}$$

where $\Delta \boldsymbol{x}_i^N = \boldsymbol{x}_N - \boldsymbol{x}_i$ is the Relative Position Increment (RPI) from time t_i to t_N. The $\boldsymbol{p}_r$ is the position of the physical beacon. Note that $\boldsymbol{p}_{v,N} = \boldsymbol{p}_r$ as $\Delta \boldsymbol{x}_N^N = 0$.

According to the quadratic nonlinear equations shown in (4), the current position $\boldsymbol{x}_N$ can be determined by the Least Squares (LS) when the matrix $\mathbf{A}\mathbf{A}^{\mathrm{T}}$ is nonsingular

$$\boldsymbol{x}_N = (\boldsymbol{A}^{\mathrm{T}}\boldsymbol{A})^{-1}\boldsymbol{A}^{\mathrm{T}}\boldsymbol{B} \tag{6}$$

where $\boldsymbol{A}_i = [\boldsymbol{p}_{v,i+1} - \boldsymbol{p}_{v,i}]^{\mathrm{T}}$, $\boldsymbol{B}_i = (r_i^2 - r_{i+1}^2 + d_{i+1}^2 - d_i^2)/2$, and $d_i = ||\boldsymbol{p}_{v,i}||$. Note that $\boldsymbol{p}_{v,N+1} = \boldsymbol{p}_{v,1}$, $r_{N+1} = r_1$ and $d_{N+1} = d_1$.

Iterative closest contour point

Iterative closest contour point, a typical correlation matching method, was developed from the Iterative Corresponding Point (ICP) algorithm for image registration (Zhang et al., 2022). The feasibility of using this algorithm for gravity and terrain matching aided navigation was demonstrated by many researchers (Wang et al., 2018; Zhang et al., 2017). The fundamental concept of the ICCP matching algorithm is to find an optimal Rigid Transformation (RT) parameter $\boldsymbol{\psi}_r^+$ under the specified objective function $\mathcal{L}(\cdot,\cdot)$. The mathematical formula of ICCP is given by

$$\boldsymbol{\psi}_r^+ = \arg\min_{\boldsymbol{\psi}_r} \mathcal{L}(\boldsymbol{Y}, \mathcal{M}(\mathcal{I}_{\boldsymbol{\psi}_r}(\overline{\boldsymbol{X}}))) \tag{7}$$

where $\boldsymbol{\psi}_r \triangleq [\vartheta, \delta\boldsymbol{x}^{\mathrm{T}}] \in \mathbb{R}^3$ the RT parameter, ϑ and $\delta\boldsymbol{x}$ are the rotational and translation parameter, respectively. The RT is given by

$$\tilde{\boldsymbol{X}} \triangleq \mathcal{I}_{\boldsymbol{\psi}_r}(\overline{\boldsymbol{X}}) = \boldsymbol{R}_\vartheta \overline{\boldsymbol{X}} + \delta\boldsymbol{x} \tag{8}$$

where $\overline{\boldsymbol{X}} = [\overline{\boldsymbol{x}}_1,...,\overline{\boldsymbol{x}}_N] \in \mathbb{R}^{2\times N}$ is the indicated track. $\boldsymbol{R}_\vartheta$ is the rotation matrix w.r.t ϑ. $\tilde{\boldsymbol{X}} = [\tilde{\boldsymbol{x}}_1,...,\tilde{\boldsymbol{x}}_N]$ is the rigid track of indicated track $\overline{\boldsymbol{X}}$ determined by $\boldsymbol{\psi}_r$. The retrieval operator $\mathcal{M}(\cdot)$ retrieves the Closest Neighboring Grid (CNG) sequence of the input track according to the prestored reference map and the input track. The correction between the measured sequence $\boldsymbol{Y}$ and the retrieved sequence $\tilde{\boldsymbol{Y}} = \mathcal{M}(\tilde{\boldsymbol{X}})$ will be evaluated by the correction analysis function $\mathcal{L}(\cdot,\cdot)$, such as Mean Absolute Difference (MAD), Mean Squared Difference (MSD), Cross Correction (COR), etc.

After the optimal parameter $\boldsymbol{\psi}_r^+$ is obtained, the optimal matched track $\hat{\boldsymbol{X}}$ can be acquired by Eq. (8). In GMAN algorithms, the built-in reference map is critical for retrieval operation $\mathcal{M}(\cdot)$ to find the CNG sequence and the optimal matched track. However, developing a high-resolution and high-precision physical reference map is an essential and indispensable task, albeit time-consuming and labor-intensive. To some extent, these limitations are the underlying factors that GMAN is yet to be fully widespread.

Acoustic-beacon range-only matching aided navigation

Marine complexity, acoustic-beacon integrity, and vessel maneuverability can limit acoustic observations, and further hinder the efficacy and accuracy of the APS. The sAB-RMAN is developed for single acoustic-beacon, and its workflow is presented. The advantages of the RMAN over the GMAN are discussed in detail. Then, extensions of RAMN with multi-available acoustic-beacons (mAB-RMAN) can accommodate more application scenarios. Finally, an intuitive analysis on mAB-RMAN performance as the available acoustic beacons increase is presented.

Single acoustic-beacon RMAN (sAB-RMAN)

The SINS(DRNS)-indicated track suffers from the rigid and scaling transformation due to the irreversible accumulated errors caused by the IMU or Odometer. Thus, it is more reasonable to model the relationship between the indicated track and the reference track using an Affine Transformation (AT), which fully covers the RT when no scale error exists. Therefore, the affine rather rigid one will be adopted in RMAN.

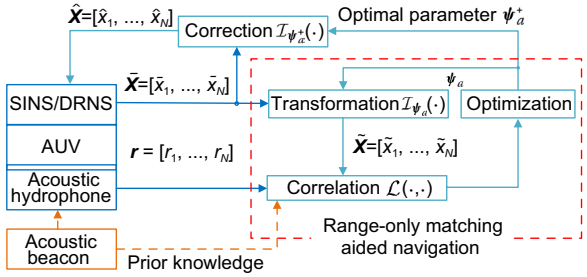

Fig. 2 The principle of sAB-RMAN

The indicated track $\overline{\boldsymbol{X}}$ will suffer an AT determined by $\boldsymbol{\psi}_a$ before feeding it into the retrieval operation $\mathcal{M}(\cdot)$. The AT is given by

$$\tilde{\boldsymbol{X}} = \mathcal{I}_{\boldsymbol{\psi}_a}(\overline{\boldsymbol{X}}) = (1+\delta\kappa)\boldsymbol{R}_\vartheta \overline{\boldsymbol{X}} + \delta\boldsymbol{x} \tag{9}$$

where $\tilde{\boldsymbol{X}}$ is the affined track w.r.t the variable $\boldsymbol{\psi}_a \triangleq [\delta\kappa, \boldsymbol{\psi}_r] \in \mathbb{R}^4$, where $\delta\kappa$ the scale error while $\boldsymbol{\psi}_r$ is in line with the definition of Eq. (7).

Using weighted-MAD (wMAD) as the correction analysis function, the optimal $\boldsymbol{\psi}_a^+$ can be determined by solving the following problem.

$$\begin{aligned}\boldsymbol{\psi}_a^+ &= \arg\min_{\boldsymbol{\psi}_a} \mathcal{L}_{\text{wMAD}}(\boldsymbol{r}, \tilde{\boldsymbol{r}}) = \arg\min_{\boldsymbol{\psi}_a} \boldsymbol{w} \odot |\boldsymbol{r} - \tilde{\boldsymbol{r}}| \\ &= \arg\min_{\boldsymbol{\psi}_a} \boldsymbol{w} \odot \left|\boldsymbol{r} - \mathcal{M}\left(\mathcal{I}_{\boldsymbol{\psi}_a}(\overline{\boldsymbol{X}})\right)\right| \\ &= \arg\min_{\boldsymbol{\psi}_a} \sum_{i=1}^{N} w_i \left| r_i - \left\| \mathcal{I}_{\boldsymbol{\psi}_a}(\overline{\boldsymbol{x}}_i) - \boldsymbol{p}_r \right\| \right|\end{aligned} \tag{10}$$

where $\odot$ is element-wise multiply, $\boldsymbol{r} = [r_1, ..., r_N]^{\mathrm{T}}$ is the measured range sequence, and $\tilde{\boldsymbol{r}} \triangleq \mathcal{M}(\tilde{\boldsymbol{X}}) = [\tilde{r}_1, ..., \tilde{r}_N]^{\mathrm{T}}$ the retrieved range sequence w.r.t the affined track $\tilde{\boldsymbol{X}}$. $\boldsymbol{w} \in \mathbb{R}^{N\times 1}$ is the weight that can be assigned by $w_i = \frac{1}{N}$ for $i = 1, ..., N$. The retrieval operator $\mathcal{M}(\cdot)$ is given by

$$\tilde{\boldsymbol{r}} = \mathcal{M}(\tilde{\boldsymbol{X}}) = \left[\left\|\tilde{\boldsymbol{x}}_1 - \boldsymbol{p}_r\right\|, ..., \left\|\tilde{\boldsymbol{x}}_N - \boldsymbol{p}_r\right\|\right]^{\mathrm{T}} \tag{11}$$

The framework of the proposed sAB-RMAN is shown in Fig. 2. The specific range-only matching aided procedure is as follows.

Step 1 Record the slant ranges and the corresponding indicated track (including the depth difference measured by depth-meter).

Step 2 Conduct the affine transformation determined by $\boldsymbol{\psi}_a$ on the indicated track to generate candidate tracks and evaluate the correction between the measured range sequence and retrieved range sequence.

Step 3 Employ an optimization algorithm to search iteratively the global minimal value of the correlation function and find the optimal affine parameter $\boldsymbol{\psi}_a^+$. A proper function tolerance or max iteration number can be set as the stop criterion of this search process.

Step 4 Determine the optimal matching track $\hat{\boldsymbol{X}}$ with respect to $\boldsymbol{\psi}_a^+$ and correct the indicated track.

The proposed RMAN does not require expensive sensors and advanced technologies, and only a hydrophone is needed if the vehicle and acoustic beacon are time-synchronized. Moreover, the RMAN does not require the reference map, while the GMAN needs a substantial investment and effort. The retrieval operation $\mathcal{M}(\cdot)$ of the RMAN is substituted by an efficient mathematical manner rather than a database lookup. Consequently, the map resolution will no longer limit the CNG of affined tracks obtained by retrieval operation. The prior knowledge on acoustic-beacon required by the retrieval operation can be obtained through pattern recognition or acoustic communication.

The sAB-RMAN constructs a range-field akin to an electrostatic field using the beacon location for matching aided navigation. Although there are infinite matched results on the range-field due to the infinite CNG of each indicated point if no constraint is employed, the constraints among elements of the indicated track will rapidly reduce the solution space, enabling the incorporation of the ranges for matching aided purpose.

Extension of RMAN with multi acoustic-beacons

When the vehicle is moving within the effective zone of the acoustic-beacon array, multi acoustic-beacons may be available. Assuming that the acoustic-beacon location corresponding to the slant-range R_i obtained at t_i is $\boldsymbol{p}_i$, the retrieval operation of the sAB-RMAN can be substituted simply by a dynamic one.

$$\tilde{r}_i = \mathcal{M}(\tilde{\boldsymbol{x}}_i, \boldsymbol{p}_i) = \left\|\tilde{\boldsymbol{x}}_i - \boldsymbol{p}_i\right\| \tag{12}$$

The dynamic retrieval operation enables the RMAN for the scenarios with multi acoustic-beacons without additional modifications.

The matching accuracy will improve with the increased number of the acoustic-beacons. An intuitive proof, take double acoustic-beacon RMAN (dAB-RMAN) as example, is presented. As shown in Fig. 3, the initial error between the indicated position $I_i, i \in [1, N]$ and it's the reference position T_i is given by

$$\boldsymbol{e}_{0,i} = I_i T_i, \ i = 1, ..., N \tag{13}$$

When the matching aided algorithm is employed for the indicated track on the range-field #01 generated by the acoustic-beacon #01, the matched track $\hat{\boldsymbol{X}}_{\#01}$ is obtained as

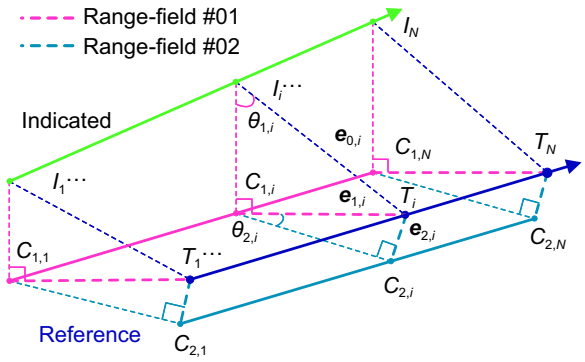

Fig. 3 Error analysis for the dAB-RMAN

$$\hat{\boldsymbol{X}}_{\#01} \triangleq \left\{ C_{1,i} \middle| I_i C_{1,i} \perp C_{1,i} T_i,\ i = 1,...,N \right\} \tag{14}$$

The remaining matching error of $I_i, i \in [1, N]$ on the range-field #01 is decreased as

$$\boldsymbol{e}_{1,i} = \boldsymbol{e}_{0,i} \times \sin\theta_{1,i}, \theta_{1,i} \in [0, \pi) \tag{15}$$

where $\theta_{1,i} = \angle C_{1,i} I_i T_i$. Obviously, $\boldsymbol{e}_{1,i} \leq \boldsymbol{e}_{0,i}$.

Applying the matching algorithm for the matched track $\hat{\boldsymbol{X}}_{\#01}$ on the range-field #02 that generated by the acoustic-beacon #02, and the rematched track $\hat{\boldsymbol{X}}_{\#02}$ can be obtained:

$$\hat{\boldsymbol{X}}_{\#02} \triangleq \left\{ C_{2,i} \middle| C_{1,i} C_{2,i} \perp C_{2,i} T_i,\ i = 1,...,N \right\} \tag{16}$$

Based on the *two-step* matching process, the matching error for indicated track can be written as

$$\boldsymbol{e}_{2,i} = \boldsymbol{e}_{1,i} \times \sin\theta_{2,i},\ \theta_{2,i} \in [0, \pi) \tag{17}$$

where $\theta_{2,i} = \angle C_{2,i} C_{1,i} T_i$. No doubt that the $|\boldsymbol{e}_{2,i}| \leq |\boldsymbol{e}_{1,i}| \leq |\boldsymbol{e}_{0,i}|$ is always hold, which means that additional acoustic-beacon can further improve the matching accuracy.

It is not difficult to generalize that the theoretical matching error of indicated point $I_i, i \in [1, N]$ with n available beacons can be expressed as

$$\boldsymbol{e}_{n,i} = \boldsymbol{e}_{0,i} \times \prod_{k=1}^{n} \sin\theta_{k,i} = \boldsymbol{e}_{n-1,i} \times \sin\theta_{n,i} \tag{18}$$

Therefore, more range-field generated by acoustic-beacon can be introduced into the mAB-RMAN to further minimize the matching error.

Improved VLBL by considering indicated-RPI error

The construction process of the virtual beacon in Eq. (5) relies entirely on the indicated RPI and physical beacon's location. The localization of underwater fixed beacons have been extensively studied and can achieve centimeter-level accuracy (Yang & Qin, 2021). The accumulated errors of SINS (or DRNS) over time will impact the accuracy of the RPI, and the indicated RPI errors will propagate directly to the virtual beacon's location, as shown in Fig. 1 with the indicated track and virtual acoustic beacon in grey. The desired performance of VLBL will only be guaranteed if the indicated RPI error is compensated. This section presents an improved single acoustic-beacon VLBL (sAB-VLBL) considering the indicated RPI error compensation. Then, the sAB-VLBL is developed to mAB-VLBL to adapted to the scenario with multi acoustic-beacons.

Improved single acoustic-beacon VLBL (sAB-VLBL)

To enhance the positional accuracy of virtual acoustic-beacons, it is crucial to initiate the error compensation of the indicated RPI. One natural and intuitive approach is to take the affine transformation with zero translation to model the relation of the true RPI $\Delta\boldsymbol{x}$ and the indicated RPI $\Delta\bar{\boldsymbol{x}}$. The i-th virtual acoustic-beacon in Eq. (5) can be rewritten as follows while considering RPI error compensation.

$$\tilde{\boldsymbol{p}}_{v,i} = \boldsymbol{p}_r + (1 + \delta\kappa)\boldsymbol{R}_\vartheta \Delta\bar{\boldsymbol{x}}_i^N. \tag{19}$$

where $\Delta\bar{\boldsymbol{x}}_i^N = \bar{\boldsymbol{x}}_N - \bar{\boldsymbol{x}}_i$ is the indicated RPI from time t_i to t_N, while $\delta\kappa$ and ϑ are the rotational and scaling error compensation factors for the indicated RPI.

Let the *to-be-solved* current position and the error compensation factors be $\boldsymbol{x}^- \triangleq [\boldsymbol{x}_N^{\mathrm{T}}, \delta\kappa, \vartheta]^{\mathrm{T}}$, which can be obtained by solving the following problem:

$$\boldsymbol{x}^+ = \arg\min_{\boldsymbol{x}^-} \boldsymbol{F}(\boldsymbol{x}^-) = \arg\min_{\boldsymbol{x}^-} \tfrac{1}{2} \sum_{i=1}^{N} \left\| f_i(\boldsymbol{x}^-) \right\|^2 \tag{20}$$

where

$$f_i(\boldsymbol{x}^-) = \left\| \boldsymbol{x}_N - \tilde{\boldsymbol{p}}_{v,i} \right\| - r_i \tag{21}$$

The abovementioned problem can be viewed as a Nonlinear Least Squares (NLS) problem. The Levenberg–Marquardt (LM) algorithm is adopted to find the optimal solution in this paper. The LM, also called the damped least squares method or Gaussian-Newtown method using a trust region approach, is a powerful means of resolving NLS problems.

Extension of the VLBL with multi acoustic-beacons

Like the RMAN extension, it is easy to extend the sAB-VLBL for multi acoustic-beacon scenario by reformulating the Eq. (21) as

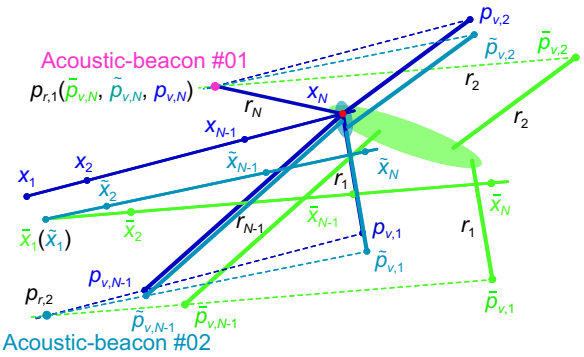

Fig. 4 The principle of dAB-VLBL

$$f_i(\boldsymbol{x}^-) = \left\| \boldsymbol{x}_N - \boldsymbol{p}_{r,i} - (1+\delta\kappa)\boldsymbol{R}_{\vartheta}\Delta\bar{\boldsymbol{x}}_i^N \right\| - r_i \quad (22)$$

where $\boldsymbol{p}_{r,i}$ is the acoustic-beacon position w.r.t the ith measured range. Takes the double acoustic-beacon VLBL (dAB-VLBL) as a particular example of mAB-VLBL for explanation, noting $\boldsymbol{p}_{r,\{1,2,\ldots,N-1,N\}} = \boldsymbol{p}_{r,\{1,2,\ldots,2,1\}}$. As shown in Fig. 4, the position of virtual acoustic-beacon directly generated by the indicated track (green) deviates significantly from the theoretical position of the virtual acoustic-beacon generated by the reference track (blue). Compared with the traditional VLBL without error compensation on the indicated RPI, the dAB-VLB will construct the virtual acoustic-beacon with higher position accuracy. It evidently leads to a more accurate outcome as shown in the shadow area.

Traditional VLBL requires the vehicles not traveling in a straight line, because it can create ambiguity (Koshaev, 2020). The accuracy of traditional VLBL will improve with the observation length N increased if the indicated-RPI is error-free. Unfortunately, the accuracy of traditional VLBL does not improve with N increased but somewhat decreases. The proposed improved VLBL with considering indicated-RPI error, especially when multi acoustic-beacons are available, reduces the requirement for vehicle maneuverability and enables higher positioning accuracy and robustness.

Performance verification

The performance of our proposed algorithms will be evaluated via simulation experiments and field trials, compared with traditional algorithms. The simulations were conducted on a computer with processor AMD Ryzen 7 5800H CPU @3.2 GHz with 32 GB of memory, all of the algorithms are implemented in Matlab 2020b. Abbreviations for different methods refer to Abbreviations section. In this paper, mAB-ICCP and mAB-RMAN are classified as match-based algorithms, with the former being the baseline for match-based comparison.

Table 1 Simulation parameters

System	Parameter	Value
DRNS	Gyro drift	0.03 (°)/h
	Gyro ARW	0.003 $(°)/h^{\frac{1}{2}}$
	Gyro frequency	100 Hz
	Initial attitude error	(1°, 0°, 1°)
	Installation error	(0.25°, 0°, 0.17°)
	Odometer scale factor	1.05
	Odometer frequency	50 Hz
Acoustic system	Ranging accuracy	2 m
	Output frequency	0.25 Hz

Similarly, the LBL-based algorithm includes the traditional VLBL, the mAB-VLBL-rot (only the rotational error is compensated), and the proposed mAB-VLBL (both the rotational and scaling error are compensated). Among them, the VLBL will play as the baseline for the LBL-based algorithm. The lowercase letter m in the notations will be substituted by the lowercase letters s and d when single and double acoustic-beacons are available. In the following discussion, unless otherwise specified, the statements with respect to the mAB-RMAN (or mAB-VLBL) are applicable to both single and double acoustic-beacon scenarios.

Simulation and field experiment setup

We adopt DRNS as the primary navigation system in the following simulation experiments. The simulation parameters for DRNS are detailed in Table 1. DRNS updates the indicated position iteratively based on Eq. (3). The gyroscope drift is 0.03 (°)/h, and the scale error of odometer is 5%. The installation angle errors between the gyroscope and the odometer are (0.25°, 0°, 0.17°). To simulate the accumulated heading error of the DRNS over time more realistically, the initial errors (1°, 0°, 1°) are set. To evaluate the effectiveness of the proposed algorithms when single and double acoustic-beacons are available, two acoustic-beacons, numbered with AB#01 and AB#02, were deployed at coordinates (32.034°, 118.020°, 30 m) and (32.050°, 18.035°, 40 m), respectively, as shown in Fig. 5. These acoustic-beacons emit fixed-format acoustic signals with frequency 0.25 Hz. The onboard hydrophone can measure the OWTT-based slant-range with ranging accuracy 2 m. The reference and DRNS-indicated track are depicted in Fig. 5, with a duration of about one hour.

The whole track is divided into five segments to cover the relationship between the track and acoustic-beacon as much as possible. They are marked as Track#01-05, abbreviated as T1-T5, with the duration [800,1300], [1400,1900], [2000,2800], [2900,3600] and [800,3600],

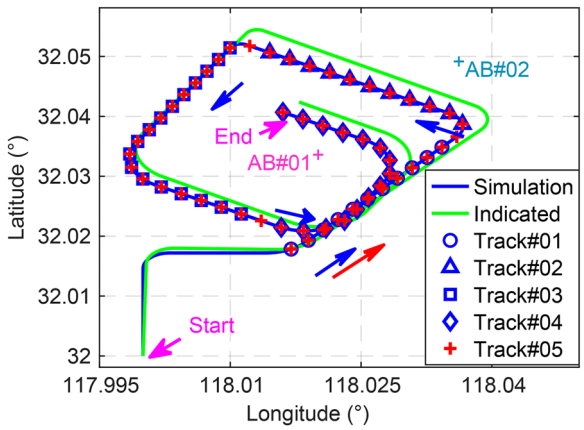

Fig. 5 Simulation track

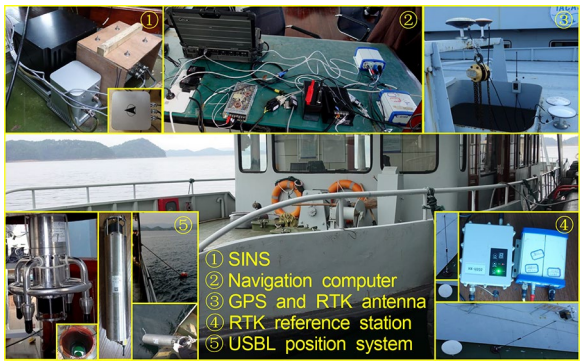

Fig. 6 The experimental instruments and environment

respectively. Note that Track#05 covers Track#01–04. This division scheme is reasonable for the performance verification on various test conditions. It is not always possible for the hydrophone to periodically acquire acoustic observations due to the complex underwater environment and vessel mobility. Hence, two scenarios, abbreviated as S1 and S2, were simulated, where S1 indicates the acoustic range received periodically while S2 randomly. For the brevity, the TnS1 and TnS2 represent that the hydrophone obtains acoustic observations periodically and randomly, respectively, under the track Tn ($n=1, \ldots, 5$).

The field experiment was conducted at Lake Qiandao, and the experimental instruments and their deployment are shown in Fig. 6. The main experimental instruments and their characteristics are detailed in Table 2. It should be noted that the USBL system is utilized to acquire the slant-range between the vehicle and the fixed acoustic-beacon rather than for USBL positioning. The relative displacement between SINS and USBL was compensated carefully. The underwater single acoustic-beacon location was determined using the method described in (He et al., 2023). Due to the experimental conditions and limitations of the reference baseline, a ship-based experiment was conducted rather than underwater AUV. In this field experiment, only single acoustic-beacon was deployed underwater. The SINS equipped with Fiber Optics Gyroscopes (FOG-SINS) was installed as the primary navigation system, operating in pure inertial mode. The drift and bias of the laser-IMU are better than 0.02 (°)/h and 50×10^{-6} g(g=9.7803 m/s^2), respectively. In addition, an ultra-precision SINS/ Global Positioning System (GPS) integrated navigation system was deployed to offer accurate reference, where the SINS is equipped with Laser gyroscopes (Laser-SINS) and GPS operating in Real-Time Kinematic (RTK) mode. Figure 7 shows the reference track and the indicated track. The whole track duration is approximately 1 700 s. Like the simulation experiments, we picked three sub-tracks with duration [344, 908], [948, 1260] and [1356, 1684], respectively, marked as Track#01–03, to evaluate the performance of algorithms under different tracks. The ESV of the simulation and lake trial is 1 473 m/s.

Table 2 Instrument parameters for the field test

Instrument	Parameters	Index
Acoustic system	Signal frequency	8–16 kHz
	Max range	3 000 m
	Ranging accuracy	1 m
	Data update rate	0.25 Hz
SINS with FOG-IMU (Laser-IMU[¶])	Gyro drift	0.02(0.003)(°)/h
	Gyro ARW	0.005(0.001) (°)/$h^{\frac{1}{2}}$
	Acc bias	50(20) × 10^{-6} g(g=9.7803 m/s^2)
	Acc VRW	10(5) × g × 10^{-6} $Hz^{-\frac{1}{2}}$
	Data update rate	100(200) Hz
GPS	Position accuracy	0.1 m @1 Hz (RTK)
PS	Accuracy	0.05 m @ 1 Hz

[¶] The SINS with Laser-IMU shown in Fig. 6.1 (the black one) is employed for acquiring high-precision reference information

In addition to the lake trial, a set of sea trial data was also collected to assess the performance of the proposed algorithms. Approximately 100 acoustic observations were obtained from two acoustic-beacons during one-hour voyage. Due to the confidentiality of this sea trial, the specific implementation procedures and equipment details are not disclosed to the public, and the positions of these acoustic-beacons, indicated track, and reference track used in the evaluation have undergone meticulous declassification procedures. Therefore, only the relative positions were provided rather than the absolute positions.

Analysis of simulation results

The statistical results of positioning accuracy and efficiency in various test conditions based on 100 times

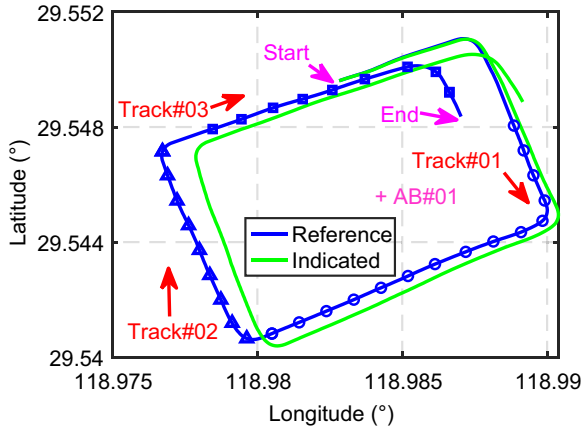

Fig. 7 The field reference and SINS-indicated track

Monte Carlo tests with different algorithms are reported in Table 3. The DRNS-indicated error is determined based on the positioning output when acoustic observation is acquired. Consequently, the indicated errors under S1 and S2 for the same track in Table 3 are slightly different. This error computation manner is suitable to evaluate the performance as these algorithms offer positioning output only when the acoustic observation is received. This approach does not introduce an explicit error as the indicated errors under S1 and S2 are identical as shown in Table 3 but facilitates more reasonable quantitative analysis of the algorithm's performance. For different test tracks under S1 and S2, the minimum and maximum mean Positioning Error (PE) of DRNS are 205.58 m and 305.02 m, respectively, and the Average PE (APE) of all the tracks is 235.60 m.

The baseline algorithm mAB-ICCP is effective for the range-only matching aided navigation. The sAB-ICCP demonstrated a substantial improvement in positioning accuracy under all test conditions. The minimum and maximum mean PE of sAB-ICCP is 42.90 m (in T1S2) and 84.51 m (in T5S2), respectively. The APE of all test conditions decreased from 235.60 m to 56.11 m, resulting in a 75.7% improvement compared with the indicated accuracy. The dAB-ICCP achieved a minimum and maximum mean PE of 33.94 m (in T2S2) and 84.52 m (in T5S1), respectively, with an APE of 50.50 m, improvement by 77.8% over indicated accuracy. Table 3 shows that dAB-ICCP reduced the APE by an additional 5.61 m compared to the sAB-ICCP, which means that more acoustic-beacons can improve the matching accuracy (improvement by 11.8% over sAB-ICCP) even though inaccurate matching model is adopted. In terms of computational efficiency, the average time consumed by the once-matching operation of the sAB-ICCP and dAB-ICCP is 0.97 s and 1.65 s, respectively. The efficiency trade-off of the dAB-ICCP brings worthwhile improvement in positioning accuracy.

The proposed mAB-RMAN achieved much better accuracy than the mAB-ICCP while maintaining an acceptable computational efficiency. Under all the test conditions, the maximum mean PE of sAB-RMAN and dAB-RMAN is only 10.19 m and 3.59 m, respectively, with minimum mean PE of only 5.37 m and 1.53 m. Undoubtedly, these are satisfactory dynamic positioning accuracy. Additionally, the APE of sAB-RMAN and dAB-RMAN is 8.40 m and 2.15 m, respectively, an improvement by 96.38% and 99.04% compared to indicated accuracy. Notably, dAB-RMAN improved the positioning accuracy by 73.6% compared to sAB-RMAN. It can be concluded that the matching accuracy will be increased with more acoustic-beacons available. This experimental conclusion coincides with our theoretical analysis. Most importantly, the accuracy and stability of the proposed mAB-RMAN are superior over the mAB-ICCP, which demonstrates that the matching model of *m*AB-RMAN is more reasonable and effective. In terms of computational efficiency, the average time consumed by the sAB-RMAN and dAB-RMAN is 1.61 s and 2.53 s, respectively. Considering the significant improvement in positioning accuracy, mAB-RMAN is completely acceptable for navigation computers though the computational efficiency is lower.

In addition, since the Cumulative Distribution Function (CDF) can describe the probability distribution of random variables and is the integral of the probability density function, it also used as one of the positioning performance metrics to evaluate the PE of different methods. The average CDF curves of 100 Monte Carlo tests for different methods under different conditions are shown in Fig. 8. From these figures, it can be verified that the proposed mAB-RMAN can reduce significantly the PE over DRNS and mAB-ICCP under all conditions. Take the Track#05 as example, Fig. 9 plots the positioning error of 100 Monte Carlo tests. The max PE of sAB-RMAN and dAB-RMAN is less than 30 m and 10 m, respectively, while the mAB-ICCP over 150 m. The above validation and analysis demonstrates that the mAB-RAMN is effective and accurate.

The statistical results of APE for LBL-based algorithms are plotted in Fig. 10(a)–(h). To investigate the inherent correlation between the positioning accuracy and the observation length *N*, we tested the parameter *N* in Eq. (4), which ranges from 15 to 30. The VLBL indicates lower APEs on complex maneuvering tracks (such T4) than smoother ones (such T1) when single acoustic-beacon is available. This finding is consistent with the fundamental requirement of the VLBL, which relies on vehicle maneuverability. Therefore, applying the

Table 3 The position accuracy and efficiency performance of different algorithms under various conditions

Test condition	Results of DRNS	Results of mAB-ICCP				Results of mAB-RMAN			
	Error (m)	Error (m) [a]	Error (m) [b]	Time (s) [a]	Time (s) [b]	Error (m) [a]	Error (m) [b]	Time (s) [a]	Time (s) [b]
T1S1	205.58 ± 39.76	43.18 ± 22.55	36.45 ± 19.63	0.86 ± 0.13	0.89 ± 0.05	**8.19 ± 2.23**	**3.39 ± 0.50**	1.50 ± 0.36	2.47 ± 0.46
T1S2	208.93 ± 41.35	42.90 ± 22.79	37.51 ± 21.30	0.81 ± 0.11	0.72 ± 0.05	**9.18 ± 2.43**	**3.59 ± 0.78**	1.43 ± 0.33	1.97 ± 0.40
T2S1	304.83 ± 3.88	45.18 ± 26.39	34.44 ± 22.29	0.87 ± 0.11	1.31 ± 0.28	**8.61 ± 1.33**	**1.43 ± 0.73**	1.62 ± 0.34	2.00 ± 0.43
T2S2	305.02 ± 3.93	45.12 ± 26.90	33.94 ± 23.18	0.79 ± 0.09	1.18 ± 0.30	**9.35 ± 1.50**	**1.54 ± 0.81**	1.43 ± 0.32	1.75 ± 0.39
T3S1	220.93 ± 51.30	60.99 ± 35.14	55.27 ± 31.63	0.95 ± 0.11	1.43 ± 0.27	**10.19 ± 1.42**	**2.10 ± 0.78**	1.81 ± 0.43	2.64 ± 0.54
T3S2	223.24 ± 52.55	62.13 ± 34.07	56.40 ± 32.52	0.85 ± 0.12	1.18 ± 0.21	**10.10 ± 1.56**	**2.28 ± 0.95**	1.60 ± 0.38	2.13 ± 0.45
T4S1	217.66 ± 37.75	47.45 ± 22.56	40.90 ± 22.91	0.84 ± 0.10	1.40 ± 0.22	**5.37 ± 1.99**	**1.85 ± 0.52**	1.22 ± 0.20	1.96 ± 0.45
T4S2	217.89 ± 38.51	46.94 ± 23.08	42.87 ± 22.24	0.75 ± 0.09	1.27 ± 0.30	**5.77 ± 2.26**	**1.93 ± 0.60**	1.15 ± 0.25	1.71 ± 0.41
T5S1	235.61 ± 56.01	82.66 ± 38.87	84.52 ± 39.47	1.94 ± 0.23	2.92 ± 0.28	**8.85 ± 2.84**	**1.70 ± 0.65**	2.80 ± 0.34	5.05 ± 0.53
T5S2	237.38 ± 56.17	84.51 ± 42.95	82.69 ± 31.16	1.08 ± 0.12	4.18 ± 1.45	**8.37 ± 2.79**	**1.65 ± 0.65**	1.52 ± 0.19	3.65 ± 0.68
Average	235.60	56.11	50.50	0.97	1.65	**8.40**	**2.15**	1.61	2.53
Improvement (%)		75.76	77.99 (11.77)	–	–	96.38	99.04 (73.64)	–	–

Bold values mean the performance is better than other methods under the same test condition

[a] Single acoustic-beacon available; [b]double acoustic-beacons are available

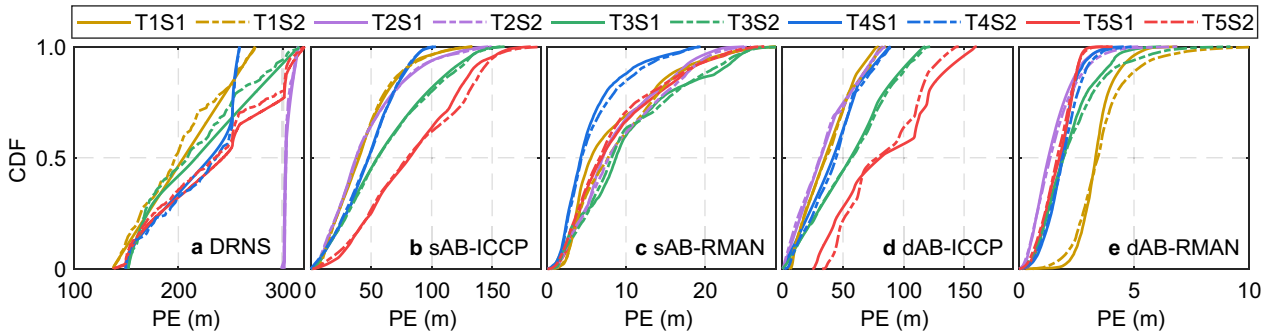

Fig. 8 The CDFs of PE for the **a** DRNS; **b** sAB-ICCP; **c** sAB-RMAN; **d** dAB-ICCP and **e** dAB-RMAN

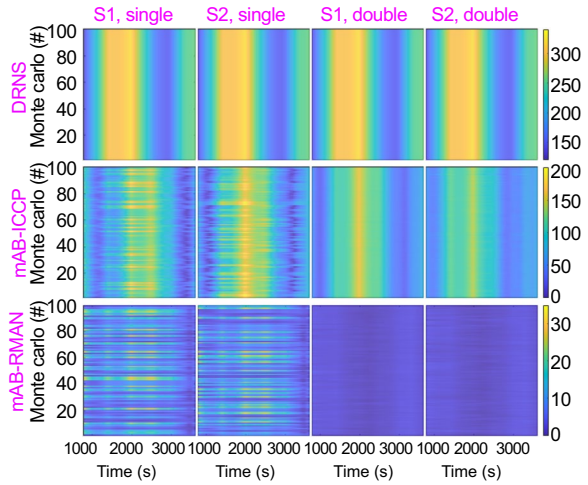

Fig. 9 Positioning error results of 100 times Monte Carlo experiments for Track#05 under various test conditions. First row is the Monto Carlo result of DRNS; the second row is the Monto Carlo result of mAB-ICCP; the last row is the Monto Carlo result of mAB-RMAN. Each column is under the same test condition

LBL-based algorithm in a vehicle moving along a straight line may deliver a lower convincing outcome.

Additionally, under different test conditions (with the same N and acoustic-beacons), the positioning accuracy of VLBL and mAB-VLBL-rot is significantly affected by the effectiveness of the acoustic-beacon, i.e., whether the hydrophone can periodically receive acoustic observations has a direct impact on these two methods. Approximately, these two algorithms will exhibit better positioning accuracy if acoustic observation can be acquired periodically, indicating that the application requirements for VLBL and mAB-VLBL-rot are more stringent. There are two reasons for this phenomenon. Firstly, under the same track, periodic working will obtain more acoustic observations for positioning, which will inevitably impact the positioning accuracy. On the other hand, using the same N to solve the current position requires walking a longer distance in S2, which undoubtedly leads to more uncertainty in the location of virtual beacons, resulting in a larger solution space, as shown in Fig. 4. However, the positioning accuracy of the proposed mAB-VLBL algorithm does not exhibit the aforementioned phenomenon. This is entirely attributed to the reasonable error compensation for the indicated RPI. Moreover, this improvement brings considerable benefits to our positioning accuracy. It can be concluded that under any condition, mAB-VLBL not only has better positioning accuracy but also better adaptability.

Table 4 summarized the statistical results of the APE and efficiency of the LBL-based algorithms under different N. The APEs of the baseline VLBL are 28.82 m and 10.08 m, which means the decline of 87.96% and 96.00% compared to DRNS-indicated error. Besides this, when single and double acoustic-beacons are available, the time consumed by the single-point positioning of VLBL is 21 ms and 23 ms, respectively. It is worth noting that the single-point positioning time of the sAB-VLBL-rot is longer by over 65.85% than that of the VLBL, but the expected improvement in accuracy caused by the rotational compensation of indicated-RPI is only observed under certain testing conditions, as shown in Fig. 10. In other words, only performing rotational compensation for the virtual beacons does not guarantee a complete improvement in positioning accuracy and may even lead to a slight degradation. This phenomenon can be attributed to the pronounced scale error (5%) that we have set, and this unexpected phenomenon will significantly diminish in practical application, just as shown in the field result in following.

The proposed mAB-VLBL offers significant improvement in accuracy compared to both VLBL and mAB-VLBL-rot, with APE only 7.45 m and 3.50 m, respectively, which improves the DRNS-indicated accuracy by 96.88% and 98.75%. In addition, dAB-VLBL can further enhance the positioning accuracy by 53% compared to sAB-VLBL. Compared to mAB-VLBL-rot, the additional compensation on scale factor in the

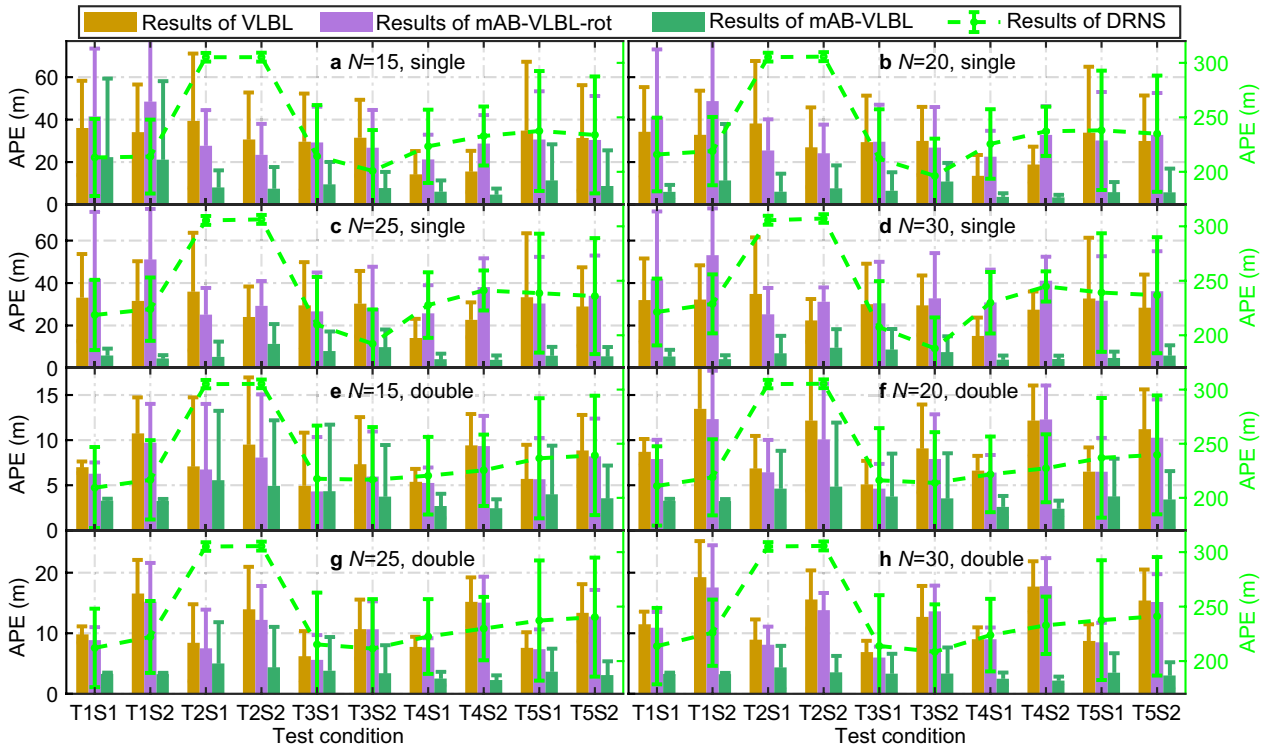

Fig. 10 The APE comparison of different algorithms under **a** $N=15$; **b** $N=20$; **c** $N=25$; and **d** $N=30$ with single acoustic beacon is available; and **e** $N=15$; **f** $N=20$; **g** $N=25$; **h** $N=30$ with double acoustic beacons are available

Table 4 The statistics result of APE and efficiency for different algorithms

	Methods		Results of $N=15$	Results of $N=20$	Results of $N=25$	Results of $N=30$	Average
APE (m)	DRNS	Mean [a]	238.03	239.00	239.96	240.88	239.47 m
		Mean [b]	239.24	239.62	240.16	240.84	239.96 m
	VLBL	Mean [a]	29.71	28.77	28.34	28.46	28.82 (↓87.96%)
		Mean [b]	7.60	9.19	10.95	12.57	10.08 (↓96.00%)
	mAB-VLBL-rot	Mean [a]	30.80	31.43	33.06	35.45	32.68 (↓86.35%)
		Mean [b]	6.95	8.47	10.29	12.04	9.44 (↓96.27%)
	mAB-VLBL	Mean [a]	**10.70**	**6.67**	**6.38**	**6.07**	**7.45 (↓96.88%)**
		Mean [b]	**3.78**	**3.54**	**3.46**	**3.22**	**3.50 (↓98.75%)**
Time (s)	VLBL	Time [a]	0.016	0.026	0.020	0.024	0.021 s
		Time [b]	0.022	0.024	0.021	0.023	0.023 s
	mAB-VLBL-rot	Time [a]	0.032	0.038	0.033	0.036	0.034 (↑65.85%)
		Time [b]	0.034	0.038	0.036	0.038	0.036 (↑61.08%)
	mAB-VLBL	Time [a]	0.042	0.045	0.042	0.043	0.043(↑108.51%)
		Time [b]	0.041	0.045	0.042	0.044	0.043 (↑91.22%)

Bold values mean the performance is better than other methods under the same test condition

[a] Single acoustic beacon is available; [b]double acoustic beacons are available

mAB-VLBL brings about substantial gains in accuracy, more than 77.1% and 62.9% when single and double acoustic-beacons are available, respectively. Although the efficiency of mAB-VLBL is only half of that of the baseline, this reduction in efficiency will not cause an intolerable burden on the navigation computer as its single-point positioning time is only 43 ms, which is completely tolerable when compared to the acoustic

observation rate (typically 0.1–1 Hz). This compromise in efficiency ensures a higher accuracy.

Another significant finding revealed from Table 4 is that the positioning accuracy of VLBL and mAB-VLBL-rot is not improved with N increased, even though the latter incorporates the rotational compensation on the indicated-RPI. Only the proposed mAB-VLBL shows consistence with expectation. The explanation for this phenomenon lies in the inherent rotational and scaling errors in indicated RPI, which will propagate into virtual acoustic-beacons. Although the redundant observations can increase reliability, the VLBL and mAB-VLBL-rot still fail to eliminate (ultimately) the position errors of the virtual beacons from indicated RPI. In contrast, the mAB-VLBL simultaneously tackles rotational and scaling error corrections on indicated-RPI, theoretically improving the accuracy of virtual beacon positions. Consequently, increasing the observations will improve the positioning accuracy, highlighting the advantage of the proposed method. This result is theoretically explainable and consistently supported as well by the following field trial data.

Analysis of the field test results

Figure 11 depicts the positioning results and error curves for the lake trail, and the corresponding statistical results are presented in Table 5 (left part). For the lake trail, all the LBL-based algorithms were compared with observation length $N=15$.

The match-based baseline sAB-ICCP successfully reduced the mean PE for Track#01–03 from 54.93 m, 98.18 m, and 163.93 m to 17.57 m, 4.40 m and 22.66 m,

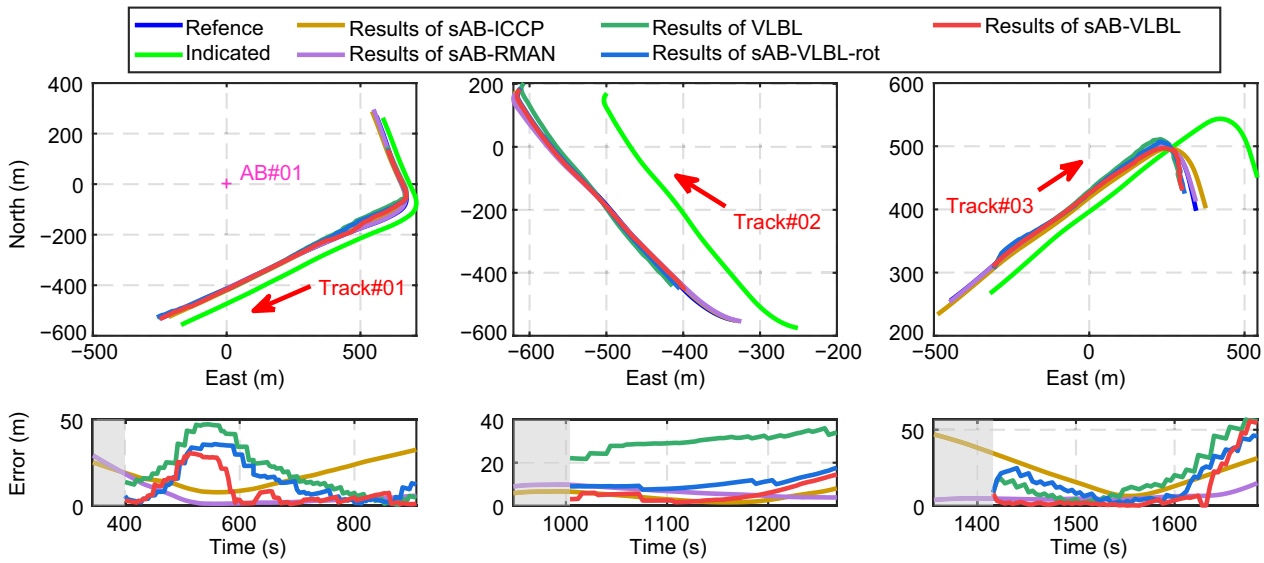

Fig. 11 Positioning results (**Up**) and errors (**Down**) of different algorithms in the lake trial

Table 5 The positioning accuracy of different algorithms for the field experiments

Method	Results of the lake trial (m) [a]			Results of the sea trail (m) [b]		
	Track#01	Track#02	Track#03	$N=10$	$N=15$	$N=20$
Indicated	54.93 ± 17.31	98.18 ± 8.56	163.92 ± 22.52	705.74 ± 40.15		
mAB-ICCP	17.57 ± 7.15	**4.40 ± 1.91**	22.66 ± 11.72	46.53 ± 26.27 (↓93.41%)		
mAB-RMAN	**6.41 ± 7.06**	6.81 ± 2.12	**5.69 ± 2.27**	**0.53 ± 0.15** (↓99.92%)		
VLBL	20.19 ± 14.27	29.90 ± 3.54	19.13 ± 16.73	23.32 ± 12.40	36.36 ± 15.93	45.11 ± 16.18
mAB-VLBL-rot	13.91 ± 11.44	10.39 ± 2.42	16.19 ± 12.90	13.40 ± 7.70	20.31 ± 11.82	26.18 ± 13.01
mAB-VLBL	**8.69 ± 9.30**	**5.49 ± 3.44**	**8.94 ± 15.35**	**6.92 ± 6.80**	**4.50 ± 2.81**	**3.48 ± 2.81**

Bold values mean the performance is better than other methods under the same test condition

[a] Single acoustic-beacon is available and the LBL-based algorithms take $N=15$; [b] double acoustic-beacons are available

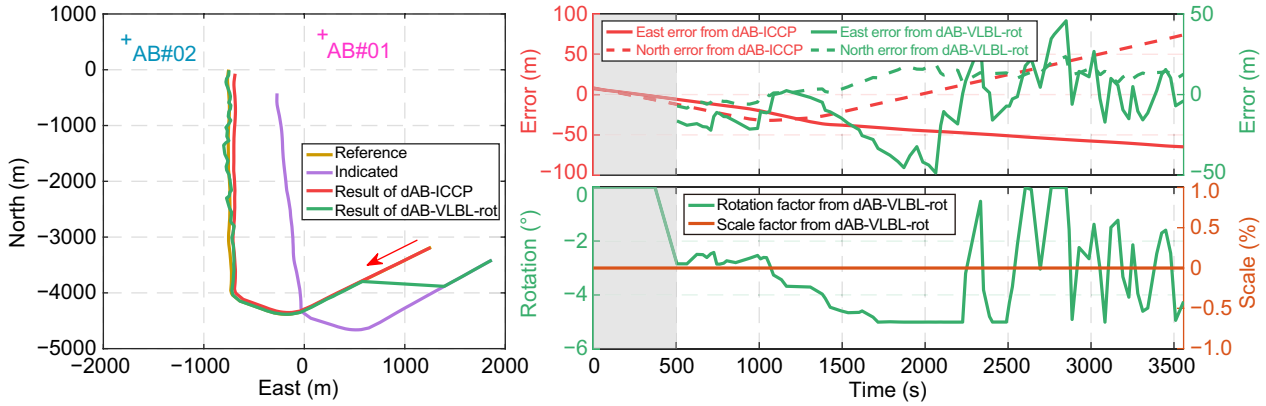

Fig. 12 Position results of the dAB-ICCP and dAB-VLBL-rot with $N = 15$ in sea trial

respectively, with an average reduction of 83.23%. The proposed sAB-RMAN outperforms sAB-ICCP by achieving lower mean PE of 6.41 m, 6.81 m, and 5.69 m, respectively. The sAB-RMAN achieves an impressive mean PE reduction of 92.64% compared to the indicated accuracy, with a minimum decrease of 88.33% (Track#01) and a maximum of 96.53% (Track#03). Furthermore, the sAB-RMAN improves the positioning accuracy by 27.87% compared to sAB-ICCP. It is important to note that the sAB-ICCP achieved a higher positioning accuracy than sAB-RMAN in the Track#02, and the characteristics of the track may potentially explain this result. However, it exhibits significantly lower stability across different test tracks than the *s*AB-RMAN. The results of the match-based algorithms in both simulation and field tests demonstrate that incorporating the affine transformation into RMAN will significantly improve positioning accuracy compared to rigid one. This finding highlights the necessity and effectiveness of affine correction for the indicated track.

In comparison of LBL-based methods, the proposed sAB-VLBL demonstrates superior performance. The mean PE is only 8.69 m, 5.48 m, and 8.94 m, with an average reduction of 91.04% compared to indicated error. Furthermore, VLBL and sAB-VLBL-rot show average reductions of 73.71% and 84.73% compared to indicated error, respectively. Due to the compensation on the indicated RPI, both sAB-VLBL-rot and sAB-VLBL achieve higher positioning accuracy than the baseline. Compared with the baseline and sAB-VLBL-rot, the sAB-VLBL can further enhances average positioning accuracy by 63.94% and 43.15%, respectively. The additional compensation on scale factors compared to sAB-VLBL-rot enhances accuracy by minimum 38.09% (on Track#01) and maximum 47.16% (for the Track#02), respectively. Note that VLBL performed worst in Track#02, demonstrating that applying the traditional VLBL for a vehicle moving along a straight line will deliver a less convincing outcome. Given the inability of underwater vehicles to navigate in perfectly straight paths, the benefits of compensating for

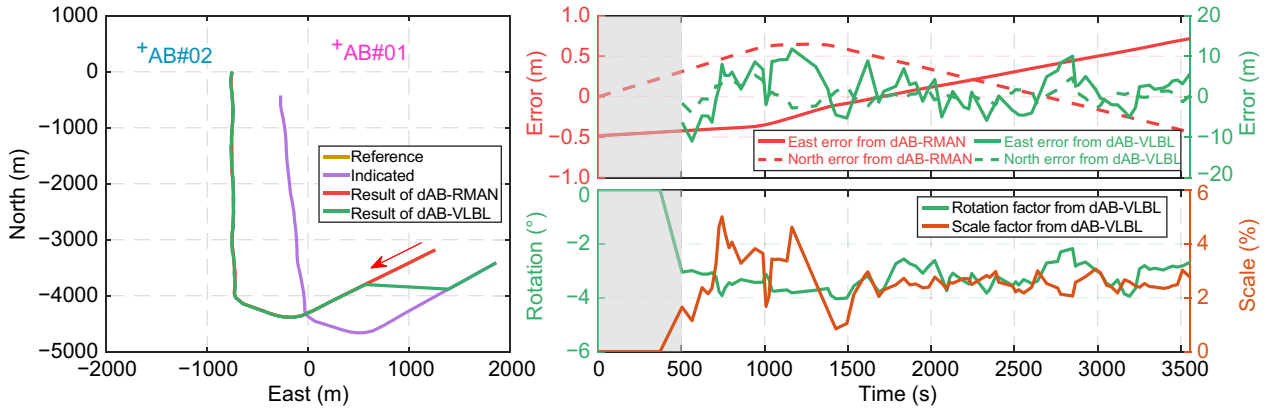

Fig. 13 Position results of the proposed dAB-RMAN and dAB-VLBL with $N = 15$ in sea trial

indicated-RPI are immediately apparent, and this assertion can be easily derived from Table 5. These evidences and analysis demonstrate the effectiveness and superiority of the proposed mAB-VLBL.

The results of the sea trial presented in Table 5 (right part) show that the proposed algorithms can correct the indicated RPI effectively, significantly improving the performance over the baseline. The match-based baseline dAB-ICCP can reduce the indicated error by 93.41%, while the proposed dAB-RMAN can reduce up to 99.92%, which means a positioning accuracy close to the acoustic measuring accuracy. The baseline dAB-ICCP achieved a positioning error of 46.53 m, even though it is already a good improvement on the indicated error (705.74 m). This residual error in dAB-ICCP can be attributed to the 2.59% scale error (refer to dAB-RMAN), which has not been compensated yet. In the LBL-based comparison, the dAB-VLBL holds a clear advantage over the VLBL and dAB-VLBL-rot, with an impressive mean PE reduction of 99.30% compared to the indicated accuracy. The results of the positioning, positioning error, and correction parameters for the match-based and LBL-based algorithms are reported in Figs. 12 and 13, where the LBL-based algorithm is employed with $N=15$. It can be observed that the estimated error compensation coefficients of LBL-based algorithms closely align with the match-based ones, though they appear to be somewhat non-smooth. It should be acknowledged that we do not report the point-by-point matching algorithm in this paper, but a sequence-based matching one. However, this is already included in our agenda.

A more accurate positioning solution cannot be accomplished solely by increasing the observation length N without compensating the indicated RPI. This assertion is also supported by the positioning results of LBL-based algorithms presented in Table 5 (right part) for different N. Surprisingly, VLBL and dAB-VLBL-rot perform worse despite a bigger N is adopted to address the current position. These sea trial evaluations are consistent with the statistical results in Table 4 exactly. This outcome can be explained as that the position of the virtual beacons is erroneous as it is derived directly from the inaccuracy indicated RPI. The dAB-VLBL-rot only compensates for the rotational error of the RPI, yet it improves accuracy by 42.8% compared to VLBL. The proposed dAB-VLBL attains an average gain of 83.4% and 70.9% in accuracy compared to the baseline and dAB-VLBL-rot, respectively. Furthermore, with an increase in observations, the desired positioning accuracy can be obtained. This indicates that compensating for the indicated RPI will improve the accuracy of the virtual beacons, thereby naturally getting accurate positioning.

Conclusion

This paper investigated two classes, match-based and LBL-based, of underwater inertial error rectification algorithms with limited acoustic observations. Firstly, a novel match-based mAB-RMAN algorithm is proposed for acoustic beacon range-only navigation by introducing the matching-aided concept. Furthermore, an improved LBL-based mAB-VLBL algorithm that considers the indicated RPI error is proposed. Comprehensive simulation and field tests were conducted to verify the effectiveness and accuracy of the proposed methods, including sAB-RMAN, dAB-RMAN, sAB-VLBL, and dAB-VLBL. We arrive at the following conclusions.

1. The mAB-RMAN gives a novel perspective for acoustic beacon range-only navigation and is effective for inertial error rectification. The mAB-RMAN achieved excellent performance compared to the baselines. In simulation, the sAB-RMAN and dAB-RMAN improved accuracy by 96.38% and 99.04%, respectively. In field tests, they performed well with accuracy improvements by 92.64% and 99.92%, respectively.
2. The mAB-LBL demonstrated excellent ability in compensating for the indicated RPI, which can significantly improve positioning accuracy by using more acoustic observations, but not for VLBL. The proposed mAB-LBL method exhibited superior in terms of accuracy and stability compared to the baseline. In simulation, the sAB-VLBL and dAB-VLBL achieved an improvement of 96.88% and 98.75%, respectively. In field tests, their improvement is 91.04% and 99.30%, respectively.

We are convinced that the proposed algorithms have a great potential in acoustic beacon range-only navigation. Future work is as follows.

1. Collecting more extensive field datasets to facilitate a more comprehensive assessment of algorithm performance.
2. A more appropriate matching algorithm for range-only matching-aided navigation will be explored while considering real-time performance.

Abbreviations

GNSS	Global navigation satellite system
INS	Inertial navigation system
SINS	Strapdown inertial navigation system

DRNS	Dead reckoning navigation system
DVL	Doppler velocity log
RTT	Round-trip time
OWTT	One-way travel time
APS	Acoustic positioning system
LBL	Long baseline
USBL	Ultra-short baseline
GMAN	Geophysical matching aided navigation
RMAN	Range-only matching aided navigation
ICCP	Iterative closest contour point
CNG	Closest neighboring grid
SITAN	Sandia inertial terrain aided navigation
SLBL	Synthetic long baseline
VLBL	Virtual long baseline (without only error compensation for the virtual beacons)
PNT	Positioning, navigation, and timing
mAB-(sAB-, dAB-)ICCP	Multi acoustic-beacon ICCP (the prefix will substitute with sAB- and dAB- when using single and double acoustic-beacon)
mAB-(sAB-, dAB-)RMAN	Multi acoustic-beacon RMAN (the prefix will substitute with sAB- and dAB- when using single and double acoustic-beacon)
mAB-(sAB-, dAB-)VLBL	Multi acoustic-beacon VLBL (the prefix will substitute with sAB- and dAB- when using single and double acoustic-beacon, if the abbreviation is followed by a suffix 'rot', it indicates that only rotational error has been considered).
RPI	Relative position increment

Acknowledgements
The authors would like to thank Dr Enfan Lin from Peking University, and the Institute of Acoustics, Chinese Academy of Sciences for the experimental collaboration.

Author contributions
We all conceived the idea and contributed to the writing of the paper. All authors read and approved the final manuscript.

Funding
The funding was provided by Natural Science Foundation of China (Grant numbers 42004067, 62373367, 42176195)

Availability of data and materials
The data analyzed during the current study are not publicly available due to the management regulations of relevant organizations but are partly available from the corresponding author on reasonable request.

Declaration

Competing interests
The authors declare that they have no competing interests.

Received: 31 August 2023 Accepted: 21 November 2023
Published online: 05 February 2024

References

Chang, L., Bian, Q., Zuo, Y., & Zhou, Q. (2023). SINS-GNSS-integrated navigation based on group affine SINS mechanization in local-level frame. *IEEE/ASME Transactions on Mechatronics*, *28*(5), 2471–2482.

Claus, B., Kepper, J. H., Suman, S., & Kinsey, J. C. (2018). Closed-loop one-way-travel-time navigation using low-grade odometry for autonomous underwater vehicles. *Journal of Field Robotics, 35*(4), 421–434.

El-Sheimy, N., & Youssef, A. (2020). Inertial sensors technologies for navigation applications: State of the art and future trends. *Satellite Navigation, 1*(1), 2.

He, H., Tang, H., Xu, J., Liang, Y., & Li, F. (2023). A SINS/USBL system-level installation parameter calibration with improved RDPSO. *IEEE Sensors Journal*, *23*(15), 17214–17223.

Huang, Y., Zhang, Y., Xu, B., Wu, Z., & Chambers, J. A. (2018). A New adaptive extended Kalman filter for cooperative localization. *IEEE Transactions on Aerospace and Electronic Systems, 54*(1), 353–368.

Jakuba, M. V., Partan, J. W., Webster, S. E., Giaya, D., & Ramirez, C. (2021). Performance of a low-power one-way travel-time inverted ultra-short baseline navigation system. *Oceans Conference Record (IEEE)*, OCEANS 2021: San Diego – Porto, San Diego, CA, USA, 1–10.

Jankovic, U., Martinovic, L., & Zcecevic, Z. (2023). Single beacon-based AUV navigation: A comparative study of kalman filters. *2023 27th International Conference on Information Technology, IT 2023*: Zabljak, Montenegro, 1–4.

Koshaev, D. A. (2020). Multiple model algorithm for single-beacon navigation of autonomous underwater vehicle without its a priori position. Part 1. Mathematical formulation. *Gyroscopy and Navigation, 11*(3), 230–243.

LaPointe, C. E. (2006). Virtual long baseline (VLBL) autonomous underwater vehicle navigation using a single transponder. In *Masterś thesis, Massachusetts Institute of Technology and Woods Hole Oceanographic Institution*. University of Oxford.

Li, D., Xu, J., Zhu, B., & He, H. (2022). A calibration method of DVL in integrated navigation system based on particle swarm optimization. *Measurement*, *187*(October 2021), 110325.

Liu, S., Zhang, T., Zhang, J., & Zhu, Y. (2021). A new coupled method of SINS/DVL integrated navigation based on improved dual adaptive factors. *IEEE Transactions on Instrumentation and Measurement, 70*, 1–11.

Masmitja, I., Gomariz, S., Del-Rio, J., Kieft, B., O'Reilly, T., Bouvet, P. J., & Aguzzi, J. (2019). Range-only single-beacon tracking of underwater targets from an autonomous vehicle: From theory to practice. *IEEE Access, 7*, 86946–86963.

Paull, L., Saeedi, S., Seto, M., & Li, H. (2014). AUV navigation and localization: A review. *IEEE Journal of Oceanic Engineering, 39*(1), 131–149.

Qin, X., Yang, Y., & Sun, B. (2022). The refined resilient model for underwater acoustic positioning. *Ocean Engineering, 266*(P3), 112795.

Rypkema, N. R., Fischell, E. M., & Schmidt, H. (2018). *Closed-loop single-beacon passive acoustic navigation for low-cost autonomous underwater vehicles*.

Scherbatyuk, A. P. (1995). AUV positioning using ranges from one transponder LBL. *Oceans Conference Record (IEEE), 3*(3), 1620–1623.

Tang, H., Xu, J., Chang, L., Shi, W., & He, H. (2023). Invariant error-based integrated solution for SINS/DVL in earth frame: Extension and comparison. *IEEE Transactions on Instrumentation and Measurement*, *72*(Dvl), 1–17.

Vaganay, J., Leonard, J. J., Curcio, J. A., & Willcox, J. S. (2004). Experimental validation of the moving long base-line navigation concept. *2004 IEEE/OES Autonomous Underwater Vehicles*, *l*, 59–65.

Wang, B., Li, T., Deng, Z., & Fu, M. (2023). Comprehensive image matching algorithm based on local GLCM for gravity-gradient-aided navigation. *IEEE/ASME Transactions on Mechatronics*, 1–10.

Wang, D., Xu, X., Yao, Y., Zhang, T., & Zhu, Y. (2020). A novel SINS/DVL tightly integrated navigation method for complex environment. *IEEE Transactions on Instrumentation and Measurement, 69*(7), 5183–5196.

Wang, K., Zhu, T., Qin, Y., Jiang, R., & Li, Y. (2018). Matching error of the iterative closest contour point algorithm for terrain-aided navigation. *Aerospace Science and Technology, 73*, 210–222.

Wang, Y., Huang, S. H., Wang, Z., Hu, R., Feng, M., Du, P., Yang, W., & Chen, Y. (2022a). Design and experimental results of passive iUSBL for small AUV navigation. *Ocean Engineering, 248*(February), 110812.

Wang, Y., Zhang, X., Sun, S., & Wang, J. (2022b). Underwater navigation using a single beacon based on the time delays of the direct signals and the surface-reflected signals. *Applied Acoustics, 187*, 108503.

Webster, S. E., Eustice, R. M., Singh, H., & Whitcomb, L. L. (2012). Advances in single-beacon one-way-travel-time acoustic navigation for underwater vehicles. *International Journal of Robotics Research, 31*(8), 935–950.

Xu, J. (2017). Analysis on underwater PNT system and key technologies. *Navigation Positioning & Timing, 4*(1), 1–6. in Chinese.

Yang, Y. (2018). Resilient PNT concept frame. *Acta Geodaetica Et Cartographica Sinica, 47*(7), 893–898.

Yang, Y., & Qin, X. (2021). Resilient observation models for seafloor geodetic positioning. *Journal of Geodesy, 95*(7), 79.

Zhang, J., Zhang, T., Zhang, C., & Yao, Y. (2022). An improved ICCP-based underwater terrain matching algorithm for large initial position error. *IEEE Sensors Journal, 22*(16), 16381–16391.

Zhang, T., Li, Y., & Tong, J. (2017). An autonomous underwater vehicle positioning matching method based on iterative closest contour point algorithm and affine transformation. *Proceedings of the Institution of Mechanical*

Engineers Part m: Journal of Engineering for the Maritime Environment, 231(3), 711–722.
Zhao, W., Zhao, H., Liu, G., & Zhang, G. (2022). ANFIS-EKF-based single-beacon localization algorithm for AUV. *Remote Sensing, 14*(20), 1–21.
Zou, Z., Wang, W., Wu, B., Ye, L., & Ochieng, W. Y. (2023). Tightly coupled INS/APS passive single beacon navigation. *Remote Sensing, 15*(7), 1–27.

Publisher's Note